NIH Public Access
Author Manuscript
Nat Mater. Author manuscript; available in PMC 2011 March 16.

Published in final edited form as:
Nat Mater. 2009 April ; 8(4): 331–336. doi:10.1038/nmat2398.

Biodegradable luminescent porous silicon nanoparticles for *in vivo* applications

Ji-Ho Park[1,2], **Luo Gu**[1], **Geoffrey von Maltzahn**[3], **Erkki Ruoslahti**[4], **Sangeeta N. Bhatia**[3,5,6], and **Michael J. Sailor**[1,2,7,★]

[1] Department of Chemistry and Biochemistry, University of California, San Diego, La Jolla, California 92093, USA

[2] Materials Science and Engineering Program, University of California, San Diego, La Jolla, California 92093, USA

[3] Harvard-MIT Division of Health Sciences and Technology, Massachusetts Institute of Technology, Cambridge, Massachusetts 02139, USA

[4] Burnham Institute for Medical Research at UCSB, University of California, Santa Barbara, California 93106, USA

[5] Electrical Engineering and Computer Science, Massachusetts Institute of Technology, Cambridge, Massachusetts 02139, USA

[6] Division of Medicine, Brigham and Women's Hospital, Boston, Massachusetts 02115, USA

[7] Department of Bioengineering, University of California, San Diego, La Jolla, California 92093, USA

Abstract

Nanomaterials that can circulate in the body hold great potential to diagnose and treat disease[1–4]. For such applications, it is important that the nanomaterials be harmlessly eliminated from the body in a reasonable period of time after they carry out their diagnostic or therapeutic function. Despite efforts to improve their targeting efficiency, significant quantities of systemically administered nanomaterials are cleared by the mononuclear phagocytic system before finding their targets, increasing the likelihood of unintended acute or chronic toxicity. However, there has been little effort to engineer the self-destruction of errant nanoparticles into non-toxic, systemically eliminated products. Here, we present luminescent porous silicon nanoparticles (LPSiNPs) that can carry a drug payload and of which the intrinsic near-infrared photoluminescence enables monitoring of both accumulation and degradation *in vivo*. Furthermore, in contrast to most optically active nanomaterials (carbon nanotubes, gold nanoparticles and quantum dots), LPSiNPs self-destruct in a mouse model into renally cleared components in a relatively short period of time with no evidence of toxicity. As a preliminary *in vivo* application, we demonstrate tumour imaging using dextran-coated LPSiNPs (D-LPSiNPs). These results demonstrate a new type of multifunctional nanostructure with a low-toxicity degradation pathway for *in vivo* applications.

★Correspondence and requests for materials should be addressed to M.J.S. msailor@ucsd.edu.

Author contributions

J.-H.P., L.G. and M.J.S. conceived and designed the research. J.-H.P. and L.G. carried out the experiments. J.-H.P., L.G., G.v.M., E.R., S.N.B. and M.J.S. analysed the data. J.-H.P. and M.J.S. wrote the manuscript.

Additional information

Supplementary Information accompanies this paper on www.nature.com/naturematerials. Reprints and permissions information is available online at http://npg.nature.com/reprintsandpermissions.

A full description of the methods is available in Supplementary Methods.

NIH-PA Author Manuscript
NIH-PA Author Manuscript
NIH-PA Author Manuscript

NIH-PA Author Manuscript

NIH-PA Author Manuscript

NIH-PA Author Manuscript

The *in vivo* use of nanomaterials as therapeutic and diagnostic agents is of intense interest owing to their unique properties such as large specific capacity for drug loading[2], strong superparamagnetism[3], efficient photoluminescence[1,5] or distinctive Raman signatures[4], among others. Materials with sizes in the range of 20–200nm can avoid renal filtration, leading to prolonged residence time in the blood stream that enables more effective targeting of diseased tissues. Many biodegradable polymeric nanoparticles that can encapsulate hydrophilic or hydrophobic drugs have been developed for *in vivo* therapeutic applications[2,6,7], and some of them have been approved for clinical use. However, organic molecule-based nanoparticles generally require the addition of a molecular tag to enable *in vivo* monitoring by fluorescence. Although carbon nanotubes, gold nanoparticles and quantum dots have demonstrated potential for *in vivo* imaging owing to their unique optical properties[1,4,8], clinical translation has been impeded owing to concerns regarding the biodegradability of such materials[4,8,9], the toxicity of degradation by-products[10] or the toxic structural characteristics of the nanomaterials themselves[11]. Although efficient renal clearance can mitigate toxic effects, optimized formulations can leave significant residual heavy metals or other toxic constituents in mononuclear phagocytic system (MPS) organs[4,12]. Furthermore, the hydrodynamic size required for renal clearance (<5.5 nm; ref. [12]) may be too small to enable the incorporation of functional components such as multivalent targeting ligands, and rapid renal excretion reduces the time available to the nanomaterial to carry out its function. A more desirable design criterion for improving the biocompatibility of nanomaterials would involve the incorporation of controllable rates of self-destruction, through which components could be hierarchically degraded into harmless, renally cleared products after carrying out their *in vivo* function.

Electrochemically etched porous silicon has exhibited considerable potential for biological applications owing to its biocompatibility[13], biodegradability[14], encoding property for multiplexed detection[15] and tunable porous nanostructure for drug delivery[16]. Furthermore, since the discovery of photoluminescence of porous silicon in 1990 (ref. [17]), luminescent (porous) silicon nanoparticles have been produced by several methods[18–22], some of which are amenable to biological applications[21,22]. For *in vivo* use, silicon nanoparticles provide attractive chemical alternatives to heavy-metal-containing quantum dots, which have been shown to be toxic in biological environments[10]. In addition, silicon is a common trace element in humans and a biodegradation product of porous silicon, orthosilicic acid ($Si(OH)_4$), is the form predominantly absorbed by humans and is naturally found in numerous tissues. Furthermore, silicic acid administered to humans is efficiently excreted from the body through the urine[23]. Here, we show that porous silicon nanostructures with intrinsic near-infrared luminescence can be used for *in vivo* monitoring, they can be loaded with therapeutics and they can be engineered to degrade *in vivo* into benign components that clear renally within specific timescales (Fig. 1a).

Luminescent porous Si nanoparticles (LPSiNPs) were prepared by electrochemical etching of single-crystal silicon wafers in ethanolic HF solution, lift-off of the porous silicon film, ultrasonication, filtration of the formed particles through a 0.22 μm filtration membrane and finally activation of luminescence in an aqueous solution (see Supplementary Fig. S1). During the activation step, silicon oxide grows on the hydrogen-terminated porous silicon surface, generating significant luminescence attributed to quantum confinement effects and to defects localized at the $Si–SiO_2$ interface (see Supplementary Figs S2,S3)[5,18,19]. The preparation conditions were optimized to provide pore volume and surface area suitable for loading of therapeutics and long *in vivo* circulation times while maintaining an acceptable degradation rate (see Supplementary Figs S4,S5). As a result, the medium-sized (126 nm) particles prepared by electrochemical etching at $200mAcm^{-2}$ for 150 s were chosen for the study presented here. The LPSiNPs appear spherical and fairly uniform in the scanning

NIH-PA Author Manuscript

NIH-PA Author Manuscript

NIH-PA Author Manuscript

electron microscope (SEM), with a well-defined micro- and meso-porous nanostructure (Fig. 1b). The pore diameters are of the order of 5–10nm (see Supplementary Fig. S4a,b). The mean hydrodynamic size measured by dynamic light scattering is ~126 nm, consistent with the SEM measurements.

The intrinsic photoluminescence of LPSiNPs under ultraviolet excitation appears at wavelengths between 650 and 900nm (Fig. 1c), suitable for *in vivo* imaging owing to low tissue adsorption in this spectral range[24]. The materials exhibit greater photostability relative to fluorescein or the well-known near-infrared cyanine fluorophores, Cy5.5 and Cy7 (see Supplementary Fig. S6). The quantum yield of LPSiNPs in ethanol was determined to be ~10.2% (relative to Rhodamine 101 standard) (see Supplementary Fig. S7), which is in accord with previously reported values for other water-soluble luminescent silicon–silica nanoparticles[21,22]. When placed in biological solution (phosphate buffered saline (PBS), pH 7.4, 37 °C) at a mass concentration less than the solubility of silicic acid (0.1~0.2 mg ml^{-1} SiO_2; ref. [25]), LPSiNPs lose their luminescence in a short time and dissolve (Fig. 1d). A blueshift of the luminescence spectrum during degradation is indicative of a shrinking in size of the semiconductor fluorophore (see Supplementary Fig. S8). No detectable (by dynamic light scattering) LPSiNPs remain after 8 h of incubation. However, degradation is slowed by addition of a molecular or polymeric surface coating (see below).

The anti-cancer drug doxorubicin (DOX) was incorporated into the LPSiNPs (DOX-LPSiNPs, ~43.8 μg DOX per 1 mg LPSiNP) to test their potential for therapeutic applications (see Supplementary Fig. S9). The positively charged DOX molecules are bound to the negatively charged porous SiO_2 surface by electrostatic forces. Loading of DOX increases the zeta potential of the nanoparticles from −52 to −39 mV. A relatively slow release of the drug is observed at physiological pH and temperature, reaching significant levels within 8 h (Fig. 1e). The appearance of free silicic acid in solution as a function of time, indicative of degradation of the LPSiNPs, correlates with the DOX release profile. The rate of degradation of DOX-LPSiNPs is somewhat slower than bare LPSiNPs (see Supplementary Fig. S9a). We postulate that the presence of DOX molecules inhibits the nanoparticle dissolution process by slowing the rate of SiO_2 hydrolysis at the LPSiNP surface.

DOX-LPSiNPs exhibit similar or slightly greater cytotoxicity relative to free DOX, whereas bare LPSiNPs show no significant cytotoxicity (Fig. 1f). It is possible that silicic acid released by the LPSiNPs increases the cytotoxicity of DOX by decreasing local extracellular or intracellular pH(ref. [26]). In a preliminary *in vivo* study (see Supplementary Fig. S9b–d), DOX-LPSiNPs exhibited similar circulation times to bare LPSiNPs, suggesting that the adsorbed DOX molecules have no significant effect on LPSiNP circulation, in contrast to the rapid clearance observed with nanoparticles that are coated with positively charged polymer/peptide[27]. Importantly, DOX-LPSiNPs retained DOX molecules during circulation and delivered them to organs related to nanoparticle clearance such as the liver and the spleen. Previous work has shown that sequestration of DOX (in that case, in liposomes) reduces cardiotoxicity by reducing the systemic concentration of free DOX (ref. [26]).

Next, we tested biodegradability and biocompatibility of LPSiNPs *in vitro* and *in vivo*. The LPSiNP formulation is relatively non-toxic to HeLa cells *in vitro* within the tested concentration range (Fig. 2a and Supplementary Figs S4e,S5c,S10). For *in vivo* studies, LPSiNPs (20 mg kg^{-1}) were injected intravenously into mice. As with many other nanomaterials[3,4,12], the injected LPSiNPs accumulate mainly in the MPS-related organs such as the liver and the spleen (Fig. 2b). However, the LPSiNPs accumulated in the organs are noticeably cleared from the body within a period of 1 week and completely cleared in 4 weeks. The mechanism of clearance is attributed to degradation into soluble silicic acid

NIH-PA Author Manuscript

NIH-PA Author Manuscript

NIH-PA Author Manuscript

followed by excretion. This result contrasts with the slow clearance generally observed for other types of inorganic nanoparticle with diameters >5.5nm (refs [4,8,9]). Over a period of 4 weeks, the body weight of the mice injected with LPSiNPs increased slightly in a pattern similar to the control mice (Fig. 2c), indicating that the mice continue to mature without any significant toxic effects.

As the degradation of highly localized LPSiNPs may induce subsequent damage in the organs related to nanoparticle clearance, *in vivo* toxicity of LPSiNPs was further examined in kidney, liver and spleen tissues of mice 1 day and 4 weeks after LPSiNP injection. Histopathologically, no significant toxicity was observed in these tissues relative to the controls (Fig. 2d). Hepatocytes in the liver samples appeared unremarkable, and there were no inflammatory infiltrates. However, the sinusoids in between the rows of hepatocytes contained Kupffer cells (macrophages) that appeared swollen 1 day after injection. The cells returned to the normal morphology 4 weeks after injection, implying that LPSiNPs were taken up, degraded (presumably by lysosomes) and the soluble products were subsequently released from the cells. Spleen samples showed no significant change in morphology of the lymphoid follicles or in the size of the red pulp after LPSiNP injection. Kidney samples also showed no remarkable change in the morphology. Although the *in vivo* toxicity results shown here are preliminary, the LPSiNPs show promise as non-toxic biodegradable inorganic nanomaterials.

We next investigated the possibility of imaging cells *in vitro* and organs *in vivo* using the intrinsic photoluminescent properties of LPSiNPs. Significant luminescence of LPSiNPs was observed in HeLa cells using excitation wavelengths of 370, 488 and 750nm (two-photon excitation) 2 h after incubation, attributed to non-specific cellular uptake of the silica-based nanomaterials[28] (Fig. 3a and Supplementary Fig. S11). To examine their potential for *in vivo* imaging, subcutaneous and intramuscular injections of LPSiNP dispersions (20 μl aliquots, 0.1 mg ml^{-1}) into the left and right flank of a nude mouse, respectively, were administered. The mouse was imaged in a fluorescence mode (green fluorescent protein (GFP) excitation filter, 445–490nm and indocyanine green (ICG) emission filter, 810–875 nm). The signals from both injections were clearly observed without any skin autofluorescence, although the near-skin fluorescence intensity is larger than the signal emanating from deeper tissue (Fig. 3b). The fluorescence spectrum of LPSiNPs enables imaging in the near-infrared-emission range, a convenient window for *in vivo* imaging owing to the low levels of near-infrared autofluorescence of mouse skin excited with visible light[1,29].

We next examined whole-body fluorescence imaging of nude mice using LPSiNPs administered by intravenous injection. To prevent rapid degradation after injection and to increase their blood half-life, LPSiNPs were coated with the biopolymer dextran by physisorption[30] (D-LPSiNP, Supplementary Fig. S12). The coating process increased the size and zeta potential of the nanoparticles (from 125nm to 151nm and from −52mV to −43.5 mV, respectively). Bare LPSiNPs or D-LPSiNPs were injected and imaged at different time points (Fig. 3c–e). A significant fraction of the bare LPSiNPs were immediately removed by renal clearance, presumably owing to their degradation into smaller (<5.5 nm) nanoparticles[12]. The remaining nanoparticles were observed to accumulate in the liver and the spleen, consistent with the histology data discussed above.

The D-LPSiNPs exhibit a somewhat different pattern in their uptake by the MPS-related organs. These nanoparticles accumulate and degrade in the liver slowly relative to bare LPSiNPs, which is consistent with the *in vitro* degradation and *in vivo* blood half-life data (see Supplementary Fig. S12c,d). Biodistribution and histological studies of the organs collected from the same mice 24 h after injection are consistent with the whole-body

NIH-PA Author Manuscript

NIH-PA Author Manuscript

NIH-PA Author Manuscript

fluorescence imaging data (liver < spleen for LPSiNPs and liver > spleen for D-LPSiNPs) (Fig. 3f,g). These results indicate that the intrinsic luminescent properties of LPSiNPs enable the non-invasive monitoring of their biodistribution and degradation in a live animal as well as the microscopic observation of their localization in the organs.

Last, we evaluated the potential of LPSiNPs to image tumours *in vivo*. To detect and image deep-tissue diseases such as tumours by fluorescence, the excitation wavelength for the nanoparticle should be in the near-infrared range to maximize tissue penetration and minimize optical absorption by physiologically abundant species such as haemoglobin[24]. LPSiNPs emit in the near-infrared (810–875 nm) and they can be excited with red or near-infrared radiation (615–665nm or 710–760 nm) (Fig. 4a) or by two-photon near-infrared excitation (see Supplementary Fig. S11). Similar to some of the near-infrared-emitting semiconductor quantum dots[29], the quantum efficiency of LPSiNPs decreases with longer excitation wavelengths. However, the quantum yield is sufficient to enable their observation in internal organs using a conventional fluorescence imaging system.

Injection of the D-LPSiNP formulation (20 mg kg^{-1}) into a nude mouse bearing an MDA-MB-435 tumour results in passive accumulation of the nanomaterial in the tumour, as revealed in the near-infrared fluorescence image (Fig. 4b). Imaging with shorter excitation wavelengths (blue or green filter sets) results in poor differentiation of the target organ relative to the surrounding skin area (see Supplementary Fig. S13). The *ex vivo* fluorescence images and histology confirm the presence of D-LPSiNPs in the tumour (Fig. 4c,d).

This study represents the first example of the imaging of a tumour and other organs using biodegradable silicon nanoparticles in live animals, and it is important because of the biodegradability and low *in vivo* toxicity observed. The LPSiNPs injected intravenously are observed to accumulate mainly in MPS-related organs and are degraded *in vivo* into apparently non-toxic products within a few days and removed from the body through renal clearance. These larger (100 nm-scale) silicon-based biodegradable nanoparticles overcome many of the disadvantages of smaller (<5.5 nm) nanocrystals[12] such as fast clearance from circulation, low capacity for drug loading and toxicity of the residual particles that do not escape MPS uptake[4,12]. We believe the reduced *in vivo* toxicity of this multifunctional inorganic nanomaterial provides a promising pathway for clinical translation.

Methods

Preparation of LPSiNPs

Porous silicon samples were prepared by electrochemical etching of a p^{++}-type silicon wafer by application of a constant current density of 200mAcm^{-2} for 150 s in an aqueous HF/ethanol electrolyte. A freestanding film of the porous silicon nanostructure was then removed from the crystalline silicon substrate by application of a current pulse of 4mA cm^{-2} for 250 s in an aqueous HF/ethanol electrolyte. The freestanding hydrogen-terminated porous silicon film was fractured by sonication overnight, and then filtered through a 0.22 μm filtration membrane (Millipore). The nanoparticles were further incubated in deionized water for ~2 weeks to activate their luminescence in the near-infrared range. For dextran-coated LPSiNPs (D-LPSiNPs), dextran (MW~ 20000, Sigma) was physically absorbed on LPSiNPs.

Nanoparticle characterization

SEM micrographs were obtained with a Hitachi S-4800 field-emission instrument. Dynamic light scattering (Zetasizer Nano ZS90, Malvern Instruments) was used to determine hydrodynamic size and zeta potential of (D-)LPSiNPs. The photoluminescence (λ_{ex}=370 and 460nm long-pass emission filter) and absorbance spectra of (D-)LPSiNP were obtained

NIH-PA Author Manuscript

NIH-PA Author Manuscript

NIH-PA Author Manuscript

using a Princeton Instruments/Acton spectrometer fitted with a liquid-nitrogen-cooled silicon charge-coupled device detector, and a Hewlett-Packard 8452A ultraviolet–visible diode array spectrophotometer, respectively. Fluorescence images of D-LPSiNPs subjected to different excitation wavelength bands were obtained using an IVIS 200 imaging system (Xenogen).

In vitro degradation

(D-)LPSiNPs were incubated at 37 °C in PBS. An aliquot was removed at different time points and filtered with a centrifugal filter (30,000 Da molecular weight cutoff, Millipore) to remove undissolved LPSiNPs. The filtered solution was subjected to analysis by inductively coupled plasma optical emission spectroscopy (ICP-OES, Perkin Elmer Optima 3000DV). The decrease in photoluminescence of the above samples over time was also monitored.

Drug loading and cytotoxicity

LPSiNP was loaded with DOX(Sigma) in deionized water and then rinsed using a centrifugal filter. Release kinetics of DOX from DOX-loaded LPSiNPs (DOX-LPSiNPs) in PBS at 37 °C was measured by filtering out DOX-LPSiNPs from the solution at each time point using the centrifugal filter and measuring fluorescence of free DOX left in the solution at 590nm (λ_{ex} = 480 nm). For drug-mediated cytotoxicity experiments, MDA-MB-435 human carcinoma cells were incubated with LPSiNPs, DOX-LPSiNPs or free DOX for 48 h. The cytotoxicity of LPSiNPs, DOX-LPSiNPs or free DOX was evaluated using the MTT (3-(4,5-dimethyl-2-thiazolyl)-2,5-diphenyltetrazolium bromide) assay (Chemicon).

In vivo degradation, toxicity and circulation

All animal work was carried out in accordance with the institutional animal protocol guidelines in place at the Burnham Institute for Medical Research, and it was reviewed and approved by the Institute's Animal Research Committee. (D-)LPSiNPs were intravenously injected into BALB/c mice (20 mg kg^{-1}). For *in vivo* degradation studies, the mice were killed 1 day, 1 week and 4 weeks after injection, and the brain, heart, kidney, liver, lung and spleen were collected. The tissues were weighed, digested and then analysed for silicon content using ICP-OES. For the *in vivo* toxicity studies, the mass of each mouse was monitored for 4 weeks after injection and compared with control mice (PBS-injected). The sections of kidney, liver and spleen tissues collected from the mice 1 day and 4 weeks after injection were stained with haematoxylin and eosin and then examined by a pathologist.

In vivo fluorescence imaging

LPSiNPs were injected subcutaneously and intramuscularly into the left and right flank, respectively, of a nude mouse, and imaged immediately with GFP excitation (445–490 nm) and an ICG (810–875 nm) emission filter using the IVIS 200 imaging system. For systemic administration, (D-)LPSiNPs were intravenously injected into nude mice (20 mg kg^{-1}). The mice were imaged under anaesthesia several different times after injection using the IVIS 200 imaging system. The organs (bladder, brain, heart, kidney, lymph nodes, liver, lung, skin and spleen), collected 24 h after injection, were also imaged. The excitation filter used was GFP (445–490 nm) and the emission filter used was ICG (810–875 nm). For *in vivo* fluorescence tumour imaging, a nude mouse bearing an MDA-MB-435 human carcinoma tumour (~0.5 cm, one side of flank) was used. The tumour area was imaged under anaesthesia several different times after intravenous injection of D-LPSiNPs (20 mg kg^{-1}) using the IVIS 200 imaging system. The tumour and muscle around the tumour, collected 24 h after injection, were also imaged. The excitation filter used was Cy5.5 (615–665 nm) and the emission filter used was ICG (810–875 nm). For fluorescent histological analysis, sections of liver, spleen and tumour tissues were fixed with 4% paraformaldehyde, stained

NIH-PA Author Manuscript

NIH-PA Author Manuscript

NIH-PA Author Manuscript

with 4,6-diamidino-2-phenylindole (DAPI) and then observed with 370nm excitation and 650nm long-pass emission filter using the fluorescence microscope.

Supplementary Material

Refer to Web version on PubMed Central for supplementary material.

Acknowledgments

This work was supported by the National Cancer Institute of the National Institutes of Health through grant numbers U54 CA 119335 (UCSD CCNE), 5-R01-CA124427 (BRP) and U54 CA119349 (MIT CCNE). M.J.S., S.N.B. and E.R. are members of the Moores UCSD Cancer Center and the UCSD NanoTUMOR Center under which this work was conducted and supported by the NIH/NCI grant. J.-H.P. thanks the Korea Science and Engineering Foundation (KOSEF) for a Graduate Study Abroad Scholarship. The authors thank Melanie L. Oakes in the Hitachi Chemical Research for assistance with SEM analysis, Edward Monosov in the Burnham Institute for Medical Research for assistance with confocal and multi-photon microscopy and Nissi Varki of the Moores UCSD Cancer Center for toxicity examination of the histology samples.

References

1. Gao XH, Cui YY, Levenson RM, Chung LWK, Nie SM. *In vivo* cancer targeting and imaging with semiconductor quantum dots. Nature Biotech. 2004; 22:969–976.
2. Torchilin VP. Recent advances with liposomes as pharmaceutical carriers. Nature Rev Drug Disc. 2005; 4:145–160.
3. Lee JH, et al. Artificially engineered magnetic nanoparticles for ultra-sensitive molecular imaging. Nature Med. 2007; 13:95–99. [PubMed: 17187073]
4. Liu Z, et al. Circulation and long-term fate of functionalized, biocompatible single-walled carbon nanotubes in mice probed by Raman spectroscopy. Proc Natl Acad Sci USA. 2008; 105:1410–1415. [PubMed: 18230737]
5. Godefroo S, et al. Classification and control of the origin of photoluminescence from Si nanocrystals. Nature Nanotech. 2008; 3:174–178.
6. Sengupta S, et al. Temporal targeting of tumour cells and neovasculature with a nanoscale delivery system. Nature. 2005; 436:568–572. [PubMed: 16049491]
7. Farokhzad OC, et al. Targeted nanoparticle-aptamer bioconjugates for cancer chemotherapy *in vivo*. Proc Natl Acad Sci USA. 2006; 103:6315–6320. [PubMed: 16606824]
8. Kim D, Park S, Lee JH, Jeong YY, Jon S. Antibiofouling polymer-coated gold nanoparticles as a contrast agent for in vivo X-ray computed tomography imaging. J Am Chem Soc. 2007; 129:7661–7665. [PubMed: 17530850]
9. Ballou B, Lagerholm BC, Ernst LA, Bruchez MP, Waggoner AS. Noninvasive imaging of quantum dots in mice. Bioconjugate Chem. 2004; 15:79–86.
10. Derfus AM, Chan WCW, Bhatia SN. Probing the cytotoxicity of semiconductor quantum dots. Nano Lett. 2004; 4:11–18.
11. Poland CA, et al. Carbon nanotubes introduced into the abdominal cavity of mice show asbestos-like pathogenicity in a pilot study. Nature Nanotech. 2008; 3:423–428.
12. Choi HS, et al. Renal clearance of quantum dots. Nature Biotech. 2007; 25:1165–1170.
13. Bayliss SC, Heald R, Fletcher DI, Buckberry LD. The culture of mammalian cells on nanostructured silicon. Adv Mater. 1999; 11:318–321.
14. Canham LT. Bioactive silicon structure fabrication through nanoetching techniques. Adv Mater. 1995; 7:1033–1037.
15. Cunin F, et al. Biomolecular screening with encoded porous-silicon photonic crystals. Nature Mater. 2002; 1:39–41. [PubMed: 12618846]
16. Salonen J, Kaukonen AM, Hirvonen J, Lehto VP. Mesoporous silicon in drug delivery applications. J Pharm Sci. 2008; 97:632–653. [PubMed: 17546667]
17. Canham LT. Silicon quantum wire array fabrication by electrochemical and chemical dissolution of wafers. Appl Phys Lett. 1990; 57:1046–1048.

NIH-PA Author Manuscript

NIH-PA Author Manuscript

NIH-PA Author Manuscript

18. Heinrich JL, Curtis CL, Credo GM, Kavanagh KL, Sailor MJ. Luminescent colloidal silicon suspensions from porous silicon. Science. 1992; 255:66–68. [PubMed: 17739915]
19. Wilson WL, Szajowski PF, Brus LE. Quantum confinement in size-selected surface-oxidized silicon nanocrystals. Science. 1993; 262:1242–1244. [PubMed: 17772645]
20. Mangolini L, Kortshagen U. Plasma-assisted synthesis of silicon nanocrystal inks. Adv Mater. 2007; 19:2513–2519.
21. Wang L, Reipa V, Blasic J. Silicon nanoparticles as a luminescent label to DNA. Bioconjugate Chem. 2004; 15:409–412.
22. Li ZF, Ruckenstein E. Water-soluble poly(acrylic acid) grafted luminescent silicon nanoparticles and their use as fluorescent biological staining labels. Nano Lett. 2004; 4:1463–1467.
23. Popplewell JF, et al. Kinetics of uptake and elimination of silicic acid by a human subject: A novel application of ^{32}Si and accelerator mass spectrometry. J Inorg Biochem. 1998; 69:177–180. [PubMed: 9629677]
24. Weissleder R. A clearer vision for in vivo imaging. Nature Biotech. 2001; 19:316–317.
25. Piryutko MM. The solubility of silicic acid in salt solutions. Russ Chem Bull. 1959; 8:355–360.
26. Minotti G, Menna P, Salvatorelli E, Cairo G, Gianni L. Anthracyclines: Molecular advances and pharmacologic developments in antitumor activity and cardiotoxicity. Pharmacol Rev. 2004; 56:185–229. [PubMed: 15169927]
27. Wunderbaldinger P, Josephson L, Weissleder R. Tat peptide directs enhanced clearance and hepatic permeability of magnetic nanoparticles. Bioconjugate Chem. 2002; 13:264–268.
28. Slowing I, Trewyn BG, Lin VSY. Effect of surface functionalization of MCM-41-type mesoporous silica nanoparticles on the endocytosis by human cancer cells. J Am Chem Soc. 2006; 128:14792–14793. [PubMed: 17105274]
29. Kim S, et al. Near-infrared fluorescent type II quantum dots for sentinel lymph node mapping. Nature Biotech. 2003; 22:93–97.
30. Suh KY, et al. Characterization of chemisorbed hyaluronic acid directly immobilized on solid substrates. J Biomed Mater Res B. 2006; 15:292–298.

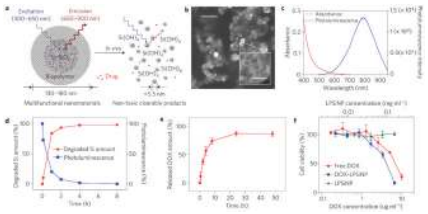

Figure 1. Characterization of LPSiNPs

a, Schematic diagram depicting the structure and *in vivo* degradation process for the (biopolymer-coated) nanoparticles used in this study. **b**, SEM image of LPSiNPs (the inset shows the porous nanostructure of one of the nanoparticles). The scale bar is 500nm (50nm for the inset). **c**, Photoluminescence emission and absorbance spectra of LPSiNPs. Photoluminescence is measured using ultraviolet excitation (λ=370 nm). **d**, Appearance of silicon in solution (by ICP-OES) and photoluminescence intensity (λ_{ex} =370nm and λ_{em} = maximum peak intensity at each time point) from a sample of LPSiNPs (50 μg ml^{-1}) incubated in PBS solution at 37 °C as a function of time. **e**, Release profile depicting per cent of DOX from DOX-LPSiNPs released into a PBS solution as a function of time at 37 °C. Data were obtained by filtering out DOX-LPSiNPs from the solution at each time point using a centrifugal filter and measuring the fluorescence intensity of free DOX left in solution (λ_{em} = 590nm, λ_{ex} = 480 nm). **f**, Cytotoxicity of DOX-LPSiNPs, bare LPSiNPs and free DOX towards MDA-MB-435 human carcinoma cells, quantified by the MTT assay. The cells were incubated with the samples for 48 h. The error bars in **d** and **f** indicate s.d.

NIH-PA Author Manuscript NIH-PA Author Manuscript NIH-PA Author Manuscript

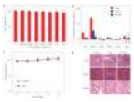

Figure 2. Biocompatibility and biodegradability of LPSiNPs

a, *In vitro* cytotoxicity of LPSiNP towards HeLa cells, determined by the calcein assay. LPSiNPs at the indicated concentrations were incubated with cells for 48 h. **b**, *In vivo* biodistribution and biodegradation of LPSiNPs over a period of 4 weeks in a mouse. Aliquots of LPSiNPs were intravenously injected into the mouse (n=3 or 4, dose=20 mg kg^{-1}). The silicon concentration in the organs was determined at different time points after injection using ICP-OES. **c**, Change in body mass of mice injected with LPSiNPs (n=3, dose=20 mg kg^{-1}) compared with PBS control (n=4). There is no statistically significant difference in the mass change between control (PBS) and LPSiNPs over a period of 4 weeks. The error bars in **a**–**c** indicate s.d. **d**, Liver, spleen and kidney histology. Livers, spleens and kidneys were collected from mice before, 1 day and 4 weeks after intravenous injection of LPSiNPs (20 mg kg^{-1}). Organs were stained with haematoxylin and eosin. The arrows indicate the LPSiNPs taken up by macrophages in the liver. The scale bar is 50 μm for all images.

NIH-PA Author Manuscript NIH-PA Author Manuscript NIH-PA Author Manuscript

NIH-PA Author Manuscript

NIH-PA Author Manuscript

NIH-PA Author Manuscript

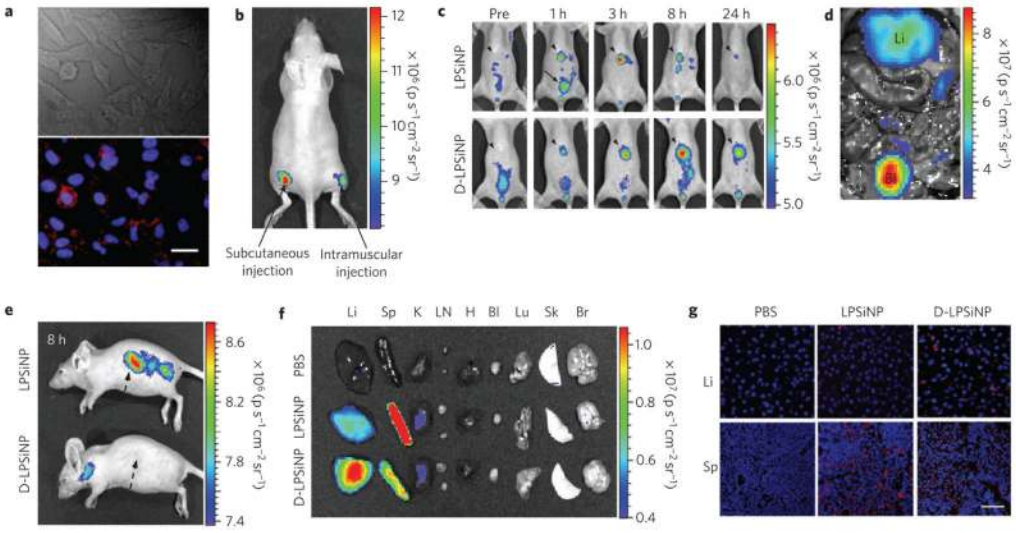

Figure 3. ***In vitro, in vivo*** **and** ***ex vivo*** **fluorescence imaging with LPSiNPs**

a, *In vitro* cellular imaging with LPSiNPs. HeLa cells were treated with LPSiNPs for 2 h and then imaged. Red and blue indicate LPSiNPs and cell nuclei, respectively. The scale bar is 20 μm. **b**, *In vivo* fluorescence image of LPSiNPs (20 μl of 0.1 mg ml^{-1}) injected subcutaneously and intramuscularly on each flank of a mouse. **c**, *In vivo* images of LPSiNPs and D-LPSiNPs. The mice were imaged at multiple time points after intravenous injection of LPSiNPs and D-LPSiNPs (20 mg kg^{-1}). Arrowheads and arrows with solid lines indicate liver and bladder, respectively. **d**, *In vivo* image showing the clearance of a portion of the injected dose of LPSiNPs into the bladder, 1 h post-injection. Li and Bl indicate liver and bladder, respectively. **e**, Lateral image of the same mice shown in **c**, 8 h after LPSiNP or D-LPSiNP injection. Arrows with dashed lines indicate spleen. **f**, Fluorescence images showing the *ex vivo* biodistribution of LPSiNPs and D-LPSiNPs in a mouse. Organs were collected from the animals shown in **c**, 24 h after injection. Li, Sp, K, LN, H, Bl, Lu, Sk and Br indicate liver, spleen, kidney, lymph nodes, heart, bladder, lung, skin and brain, respectively. **g**, Fluorescence histology images of livers and spleens from the mice shown in **c** and **f**, 24 h after injection. Red and blue indicate (D-)LPSiNPs and cell nuclei, respectively. The scale bar is 50 μm for all images.

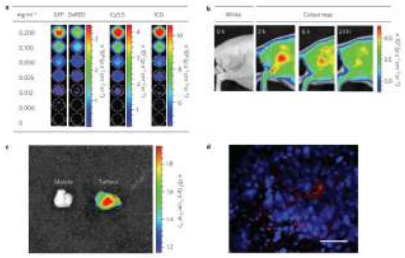

Figure 4. Fluorescence images of tumours containing D-LPSiNPs

a, Fluorescence images of D-LPSiNPs as a function of concentration using different excitation filters (GFP: 445–490nm and 1 s exposure time; Discosoma red fluorescent protein (DsRed): 500–550 nm, 2 s exposure time; Cy5.5: 615–665 nm, 8 s exposure time; ICG: 710–760 nm, 20 s exposure time). The emission filter used is ICG (810–875 nm). **b**, Representative fluorescence images of a mouse bearing an MDA-MB-435 tumour. The mouse was imaged using a Cy5.5 excitation filter and an ICG emission filter at the indicated times after intravenous injection of D-LPSiNPs (20 mg kg^{-1}). Note that a strong signal from D-LPSiNPs is observed in the tumour, indicating significant passive accumulation in the tumour by the enhanced permeability and retention (EPR) effect. **c**, *Ex vivo* fluorescence images of tumour and muscle around the tumour from the mouse used in **b. d**, Fluorescence images of a tumour slice from the mouse in **b**. Red and blue indicate D-LPSiNPs and cell nuclei (DAPI stain), respectively. The scale bar is 100 μm.

NIH-PA Author Manuscript NIH-PA Author Manuscript NIH-PA Author Manuscript